Crystallization induced enhanced emission in conformational polymorphs of a rotationally flexible molecule

Ajith R. Mallia,‡ Ramarani Sethy,‡ Vinayak Bhat and Mahesh Hariharan*

School of Chemistry, Indian Institute of Science Education and Research Thiruvananthapuram, CET Campus, Sreekaryam, Thiruvananthapuram, Kerala, INDIA 695016

Supplementary Information

Materials and methods

2,2′-Bipyridine (99%), 3-Chloroperbenzoic acid (77%) and sodium borohydride (96%) were purchased from Sigma Aldrich and used without further purification. All reactions were carried out in standard oven-dried glasswares. Inert conditions were maintained wherever necessary. Solvents were dried and distilled by standard procedures. TLC analyses were performed on precoated aluminium plates of silica gel 60 F254 (0.25 mm, Merck). Melting points (T_m) were obtained using a capillary melting point apparatus and are reported without correction. IR spectra were recorded on a Shimadzu IR Prestige-21 FT-IR spectrometer as neat KBr pellets for all the derivatives. ^{1}H and ^{13}C NMR spectra was measured on a 500 MHz and 125 MHz Bruker with AVANCE-III spectrometer respectively and 1,1,1,1-tetramethylsilane (TMS) is used as the internal standard for ^{1}H and ^{13}C NMR measurements. CHN analyses were carried out on an Elementar vario MICRO cube Elemental Analyzer. All values recorded in elemental analyses are given in percentage. High Resolution Mass Spectra (HRMS) was recorded on Agilent 6538 Ultra High Definition (UHD) Accurate-Mass Q-TOF-LC/MS system using either atmospheric pressure chemical ionization (APCI) or electrospray ionization (ESI) mode. Absorption and emission spectra was recorded on Shimadzu UV-3600 UV-VIS-NIR and Horiba Jobin Yvon Fluorolog 3, spectrofluorimeter equipped with a 450W Xe lamp and a Hamamatsu R928 photomultiplier tube respectively. Solution state relative quantum yield measurements were performed using quinine sulphate in 0.05 M H_2SO_4 as the reference (Reported quantum yield Φ = 0.546); exciting at 310 nm. The solid state quantum yield of **AMBPY** polymorphs was measured using an integrating sphere for which the accuracy was verified using tris(8-hydroxyquinolinate)aluminium (Alq_3) as a standard and is determined to be 0.37 ± 0.04 (reported quantum yield Φ_f = 0.40). Lifetime measurements were carried out in an IBH picosecond time correlated single photon counting (TCSPC) system. The detection system consisted of a micro channel plate photomultiplier (5000U-09B, Hamamastu) coupled to a monochromator (500M) and TCSPC electronics (Data station Hub including Hub-NL, NanoLED controller and pre-installed

luminescence measurement and analysis studio (FMAS) software. Pulse width of the excitation source (λ_{exc}=375 nm) was determined to be <100 ps. The fluorescence decay profiles were de-convoluted using IBH data station software version 2.1, and fitted with exponential decay, minimizing the χ^2 values. Average fluorescence lifetime values were estimated[1] using equation 1.

$$\tau_f = \frac{\alpha_1\tau_1^2 + \alpha_2\tau_2^2 + \alpha_3\tau_3^2 + \ldots}{\alpha_1\tau_1 + \alpha_2\tau_2 + \alpha_3\tau_3 + \ldots} \quad (1)$$

where α_1, α_2, and α_3 corresponds to the amplitudes corresponding to the fluorescence lifetimes τ_1, τ_2, and τ_3 respectively. The average fluorescence lifetime (τ_f) values was used to determine the radiative (k_r) and non-radiative rate constant (k_{nr})[1] as follows,

$$\Phi_f = \frac{k_r}{k_r + k_{nr}} \quad (2)$$

$$k_r = \frac{\Phi_f}{\tau_f} \quad (3)$$

$$k_{nr} = \frac{1 - \Phi_f}{\tau_f} \quad (4)$$

Φ_f, denotes solid state fluorescence quantum yield. Variations in Φ_f could be attributed to the changes in k_r or k_{nr}. An enhancement in Φ_f could be attributed to the decrease in the non-radiative (k_{nr}) rate constant.

X-ray crystallography and powder X-ray diffraction (PXRD): High-quality specimens of **AMBPY** polymorph, with approximate dimensions (0.20 × 0.15 × 0.10 mm3), were selected for the X-ray diffraction (XRD) experiments. **AMBPY-II** crystals were obtained by slow evaporation method. Accordingly, a saturated solution of amorphous **AMBPY** in benzene was prepared and transferred into a clean glass vial with large surface area. The glass vial was further covered with an aluminium foil and micro-holes were punched to ensure slow evaporation of solvent. The glass vial was kept undisturbed at room temperature to afford brown plate like crystals of **AMBPY-II**.

AMBPY-I and **III** polymorphs were obtained from liquid-liquid diffusion method. A concentrated solution of amorphous **AMBPY** in solvent (DCM for **AMBPY-I** and methanol for **AMBPY-III**) was prepared and layered with a solvent of less specific density (n-hexane in both the cases). The two liquids mixed well over time yielding crystalline **AMBPY** polymorphs having needle (**AMBPY-I**) and rhombus

(**AMBPY-III**) features. The packing efficiency for each polymorph is determined using PLATON software.[2]

Crystallographic data collected are presented in the supplementary information. Single crystals were mounted using oil (Infineum V8512) on a glass fibre. All measurements were made on a CCD area detector with graphite monochromated MoKα radiation (λ= 0.71073 Å at 298 K). The data was obatined using Bruker APEXII detector and processed using APEX2 from Bruker. All structures were solved by direct methods and expanded using Fourier techniques. The non-hydrogen atoms were refined anisotropically. Hydrogen atoms were included in idealized positions, but not refined. Their positions were constrained relative to their parent atom using the appropriate HFIX command in SHELXL-97. The full validation of CIFs and structure factors of **AMBPY** polymorphs were performed using Check CIF and found to be free from major alert level. 3D structure visualization and the exploration of the crystal packing of **AMBPY** polymorphs were carried out using Mercury 3.1.[3] PXRD spectra were recorded using an X′pert PRO (PANalytics) X-ray diffractometer. The PXRD experiments were done in a slow and continuous scan rate mode using Cu as the anode material (Kα1 = 1.5406Å).

Correlation between packing modes and solvent could be explained as follows:

Crystallisation of polymorphs from different solvents is dictated by; (i) interplay of van der Waals forces between solute and solvent molecules, (ii) hydrogen bonding interactions between solute and solvent molecules and (iii) polarity of the solvents. The strength of solute-solvent van der Waals interactions can be evaluated by the dipolar polarizability (π*). The strength of hydrogen bonding between the solvent and the solute molecules could be evaluated by the hydrogen bond donor ability (α) or the hydrogen bond acceptor ability (β) of the solvents used for crystallization. Solvents' β and π* affect the polymorph formation much lesser than α. Further, critical balance between the thermodynamic factors like temperature, solubility governs the nucleation while kinetic factors such as metastable zones, nucleation rate and supersaturation dictate crystal growth. Our ongoing interest in this aspect will focus in investigating the role of intermolecular and/or solute-solvent interactions responsible for crystallization, thereby understanding the process of crystallization.

Thermal Analysis: Thermal gravimetric analysis was carried on a SDT Q 600, thermo gravimetric analyzer (TGA). The experiments were performed under nitrogen atmosphere, by applying a heating ramp from 0 to 400 °C with a heating rate of 10 °C/min. Differential scanning calorimetric (DSC) analyses were performed in TA DSC Q20. The experiments were done under nitrogen atmosphere, by applying a heating ramp from 25 to 210 °C with a heating rate of 2 °C/min. The integral under the DSC peak, above the baseline, gives the total enthalpy change for the melting process.

$$\int \left\{\frac{dH}{dt}\right\}_{sample} dt = \Delta H_{sample} \tag{5}$$

Analysis of Chromaticity Index:[4] Coordinates (x, y, z) for chromaticity were acquired by calculating the fractional component of the tristimulus values: x = X/(X+Y+Z), y = Y/(X+Y+Z), z = Z/(X+Y+Z). X, Y, Z are the CIE 1931 tristimulus values. By convention, chromicity coordinates (x, y) denote the two dimensional plot CIE 1931 colour space chromaticity diagram.

Hirshfeld Surface Analysis:[5] Prominent intermolecular interactions present in **AMBPY** polymorphs were investigated through Hirshfeld surface analysis using Crystal Explorer 3.1. The Hirshfeld surface is defined as a volume of space where the ratio of promolecule and procrystal electron densities is equal to 0.5. The electron distribution as a result of sum of spherical atoms for the molecule (the promolecule) exceeds the corresponding sum over the crystal (the procrystal) inside the Hirshfeld surface. The exploration of intermolecular contacts is provided by mapping normalized contact distances (d_{norm}), which is a function of a closest distance from the point to the nuclei interior (di) and exterior (d_e) to the surface as well as on the van der Waals radii (r^{vdw}). Hirshfeld surface d_{norm}, displays various intermolecular interactions in terms of red, blue and white colour scheme in which red denotes short contacts, white highlights interactions operating within the range of van der Waals radii and blue represent long range contacts. 2D fingerprint plots were generated from the Hirshfeld surface by plotting the fraction of points on the surface as the function of the pair (d_i, d_e) which provide a visual summary of intermolecular contacts within the crystal.

Computational Methods: Potential energy surface was mapped employing Gaussian 09 program suite[6] using B3LYP/6-31G**+ level of theory. Materials Science Suite[7] 2015-1 provides diverse set of tools for predicting and computing reactivity and properties of chemical systems. It encompasses tools to facilitate in generating all the steps in a chemical simulation, including structure generation, property prediction followed by data analyses. The core simulation engine, Jaguar is a high performance *ab intio* quantum mechanical package commercially produced and maintained by Schrodinger Inc. Employing psuedospectral approach, Jaguar estimates the Coulomb and exchange terms, providing significant advantages of exact exchange terms. TD-DFT calculations in gas phase were performed on optimized structure of the polymorphs with Jaguar module of Schrodinger Materials Science Suite using B3LYP-D3/6-31G**+ level of theory. Frontier molecular orbital (FMO) analysis of **AMBPY** polymorphs was performed employing B3LYP-D3/6-31G**+ level of theory from crystal structure in Schrödinger Materials Science Suite using Jaguar DFT engine. Transition probability corresponding to HOMO-1 (π)

→LUMO (π*) and HOMO-2 (σ) → LUMO (π*) are positive, hence are allowed, whereas the transition probability corresponding to HOMO (n) → LUMO (π*) is possessing a negative sign hence is forbidden which is indicated in Fig. S10.

Synthesis and characterization of 2,2'-bipyridine derivatives:[8]

Synthesis of 2,2'-bipyridine-N-oxide (1A): Compound 2,2'-bipyridine in $CHCl_3$ was stirred at ice cold condition for 35 min. A solution of m-chloroperbenzoic acid in $CHCl_3$ was added to the mixture drop wise over 80 min and stirred at room temperature for 20 hours. The solution was washed with 5% aqueous Na_2CO_3, extracted with $CHCl_3$, dried over Na_2SO_4 and concentrated. The concentrated mixture was dissolved in diethyl ether and filtered to remove undissolved bipyridine-2,2'-dioxide. The filtrate was concentrated under vacuum to afford grey brown 1A with a yield of 70%. ^{1}H NMR (500 MHz, DMSO-d_6): δ = 8.76 - 8.74 (d, J = 6.75 Hz, 2H), 8.38 - 8.37 (d, J = 3.70 Hz, 1H), 8.12 - 8.10 (t, J = 4.70 Hz, 1H), 7.96 - 7.92 (t, J = 7.83 Hz, 2H), 7.51 - 7.47 (m, 2H); ^{13}C NMR (125 MHz, DMSO-d_6): δ = 149.53, 146.12, 140.46, 136.25, 132.69, 128.80, 127.89, 126.18, 125.36, 124.39; IR (KBr): 2989, 1579, 1443, 1416, 1248, 1034, 848, 723, 665 cm^{-1}; HR-MS (EI)-(m/z): 172.0682. Calcd. for $C_{10}H_8N_2O$: 172.1833; Anal. Calcd. for $C_{10}H_8N_2O$: C, 69.76; H, 4.68; N, 16.27. Found: C, 70.07; H, 4.31; N, 15.96.

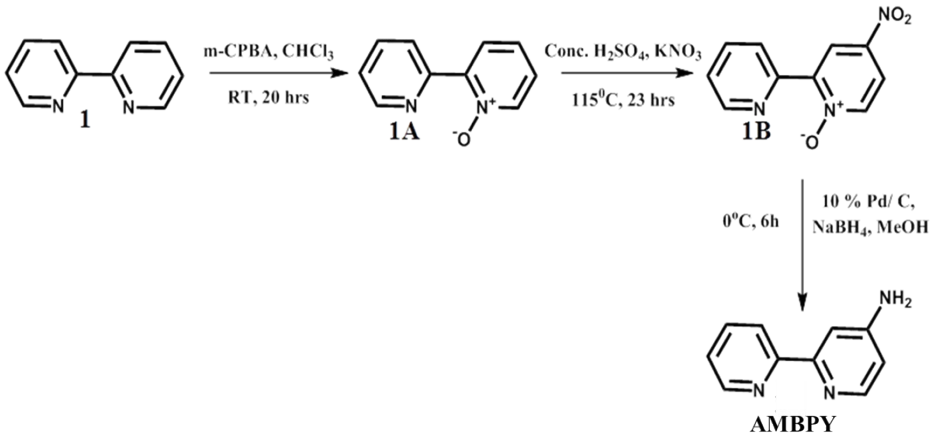

Scheme S1: Synthesis of 4-amino-2, 2'-bipyridine from 2, 2'-bipyridine.

Synthesis of 4-nitro-2,2'-bipyridine-N-oxide (1B): A solution of 16 mmol 1A and 48.1 mmol of KNO_3 in conc. H_2SO_4 were stirred at 115 °C for 23 hours. The reaction mixture was poured into ice and pH was adjusted to 8 using 16 N aq. NaOH. The obtained light yellow precipitate was filtered and washed with water. The collected precipitate was purified using column chromatography (80% ethyl acetate-petroleum ether) to obtain 1B with a yield of 50%. ^{1}H NMR (500 MHz, DMSO-d_6): δ = 8.91 - 8.89 (d, J = 3.00 Hz, 1H), 8.83 - 8.82 (d, J = 4.05 Hz, 1H), 8.79 - 8.77 (d, J = 8.05 Hz, 1H), 8.59 - 8.58 (d, J = 7.15 Hz, 1H),

8.25 – 8.23 (m, 1H)), 8.04 - 8.02 (t, J = 7.80 Hz, 1H), 7.60 - 7.58 (t, J = 6.05 Hz, 1H) ; ^{13}C NMR (125 MHz, DMSO-d_6): δ = 149.82, 147.51, 146.85, 142.24, 142.16, 136.89, 125.45, 124.62, 121.58, 119.81; IR (KBr): 3115, 3063, 1581, 1516, 1444, 1406, 1342, 1274, 1234, 1114, 895, 845, 793, 748, 659, 505 cm^{-1}; HR-MS (EI)-(m/z): 217.1603. Calcd. for $C_{10}H_7N_3O_3$: 217.1808; Anal. Calcd. for $C_{10}H_7N_3O_3$: C, 55.30; H, 3.25; N, 19.35. Found: C, 55.70; H, 3.11; N, 19.01.

Synthesis of 4-amino-2,2'-bipyridine (AMBPY): A mixture of 1B (1.22 g, 5.62 mmol) in 20 ml methanol and 10% Pd-C (200 mg) was cooled in an ice bath and stirred vigorously. To this stirring solution sodium borohydride (27.9 mmol) was added in small amounts. The mixture was stirred for 0 °C for 6 hours, and excess sodium borohydride was removed by filtration. The clear filtrate was concentrated under reduced pressure and to the residue thus obtained water was added followed by extraction with diethyl ether. The organic layer was concentrated under reduced pressure to obtain **AMBPY** with 80% yield. ^{1}H NMR (500 MHz, DMSO-d_6): δ = 8.60 - 8.59 (d, J = 4.20 Hz, 1H), 8.28 - 8.27 (d, J = 7.90 Hz, 1H), 8.08 - 8.07 (d, J = 5.50 Hz, 1H), 7.87 – 7.84 (t, J = 7.70 Hz, 1H), 7.60 – 7.59 (d, J = 1.85 Hz, 1H), 7.37 – 7.35 (t, J = 5.85 Hz, 1H),), 6.51 – 6.50 (m, 1H), 6.14 (s, 2H); ^{13}C NMR (125 MHz, DMSO-d_6): δ =156.60, 155.77, 155.63, 149.72, 149.32, 137.31, 124.05, 120.76, 109.49, 105.98; IR (KBr): 3437, 3334, 3219, 1645, 1598, 1560, 1465, 1415, 938, 792 cm^{-1}; HR-MS (EI)-(m/z): 171.0861. Calcd. for $C_{10}H_9N_3$: 171.1985; Anal. Calcd. for $C_{10}H_9N_3$: C, 70.16; H, 5.30; N, 24.54. Found: C, 69.86; H, 5.41; N, 24.31.

Table S1: Torsional angles of **AMBPY** polymorphs.

Torsional angle[a]	AMBPY-I	AMBPY-II	AMBPY-III
N(2)-C(5)-C(6)-C(7)	0.01	9.29	-19.92
N(2)-C(5)-C(6)-N(1)	-179.51	-170.81	160.21
C(4)-C(5)-C(6)-N(1)	0.93	9.45	-20.93
C(4)-C(5)-C(6)-C(7)	-179.54	-170.45	158.93
N(3)-C(8)-C(9)-C(10)	177.98	-178.60	177.96
C(6)-C(7)-C(8)-N(3)	-178.60	179.76	-178.83

[a]torsional angle is expressed in degree

Table S2: Intermolecular interactions prevailing in **AMBPY** polymorphs.

Interactions	Distance (Å)

AMBPY-I	N2•••N3–H3”	3.011
	N2•••H3’’–N3	2.151
	C1•••H3’’–N3	2.721
	C10•••H3’–N3	2.699
	N1•••H3’–N3	2.285
	C8•••H10–C10	2.657
	H9•••C9–H9	2.861
AMBPY-II	C10•••H3’–N3	2.845
	N2•••H3’–N3	2.229
	C1•••H5–C5	2.888
	N1••• H3’’–N3	2.500
	C5•••H3’’–N3	2.750
AMBPY-III	N2•••H3’–N3	1.976
	C10•••H3’–N3	2.553
	H10•••H3-N3'	2.385
	N2•••H3’’–N3	2.425
	C6•••H3’’–N3	2.560

Table S3: Percentage of intermolecular interactions present in **AMBPY** polymorphs derived from Hirshfeld surface analysis.

Interactions	**AMBPY-I (%)[a]**	**AMBPY-II (%)**	**AMBPY-III (%)**
C-H	16.9	23.6	17.7
H-H	46.7	49.8	53.1
N-H	15.8	16.5	17.5
C-C	7.4	6.4	9.2
C-N	3.3	3.0	2.3
N-N	0.4	0.7	0.2

[a] sum of all the interactions in **AMBPY-I** is estimated to be 90.6%. Void space present in the in **AMBPY-I** accounts for the remaining 9.4%, further confirming the porous nature.

Table S4: Represents packing motifs in **AMBPY** polymorphs.

	% C•••H	% C•••C	ρ= [(% C•••H))/ (% C•••C)]	motif
AMBPY-I	15.3	7.4	2.07	γ
AMBPY-II	23.6	6.4	3.68	Sandwich Herringbone
AMBPY-III	17.7	9.2	1.92	γ

Table S5: Melting temperature (T_m) and change in enthalpy (ΔH**)** values for crystalline **AMBPY** polymorphs.

	[a]T_m (°C)	[b]ΔH (kJ/mole)
AMBPY-I	126.5	17.8
AMBPY-II	126.7	17.4
AMBPY-III	126.5	19.3

[a] Melting temperature [b] Change in enthalpy during melting

Table S6: Solid state photophysical parameters of **AMBPY** polymorphs.

	Lifetime, ns (% amplitude)	Radiative rate constant (k_r x10^6 s^{-1})	Non-radiative rate constant (k_{nr} x10^8 s^{-1})
AMBPY	7.52 (8.06), 0.23 (91.94)	1.27	2.11
AMBPY-I	0.57 (6.56), 3.52 (93.44)	6.88	2.79
AMBPY-II	0.44 (78.81), 2.76 (21.19)	30.59	4.96
AMBPY-III	0.33 (89.46), 3.14 (10.54)	14.45	5.41

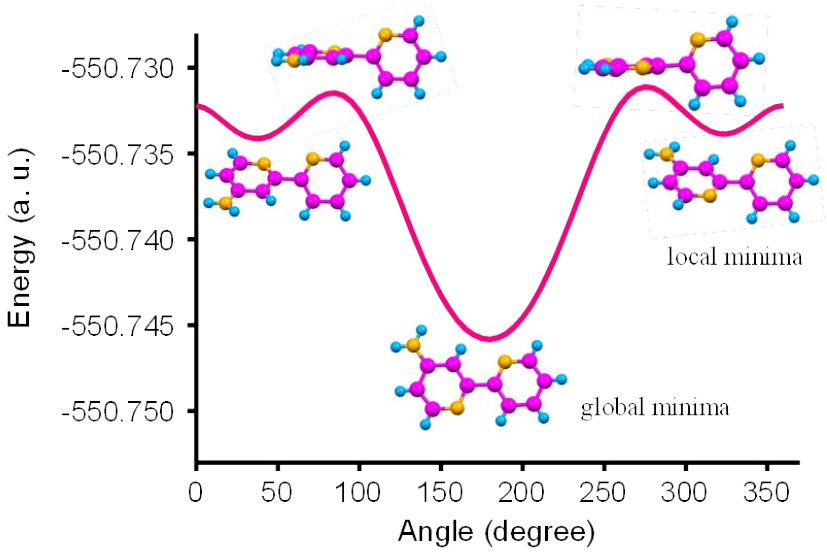

Figure S1: Potential energy surfaces for **AMBPY** with their local and global maxima and minima.

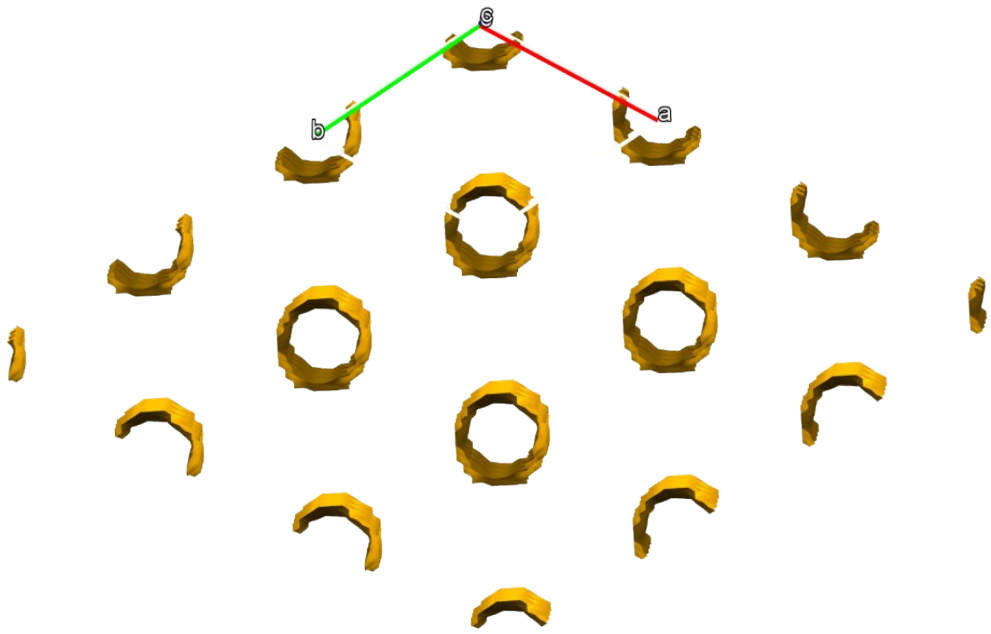

Figure S2: Three dimensional pore distribution in **AMBPY-I** polymorph.

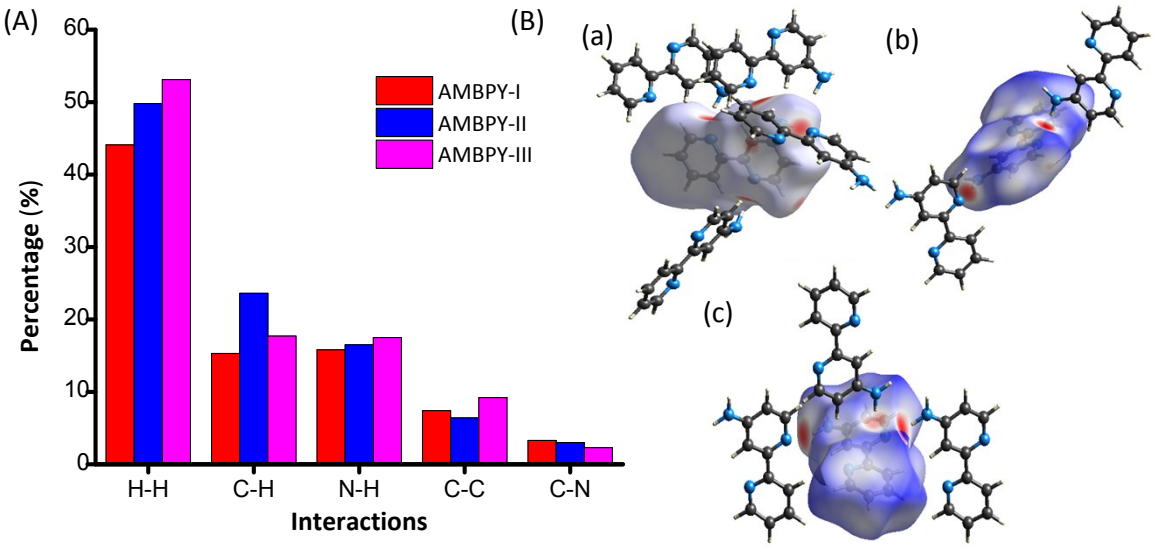

Figure S3: (A) Histogram representing various intermolecular interactions present in **AMBPY** polymorphs and (B) Hirshfeld surface (d_{norm}) analyses of (a) **AMBPY-I**, (b) **AMBPY-II** and (c) **AMBPY-III** respectively.

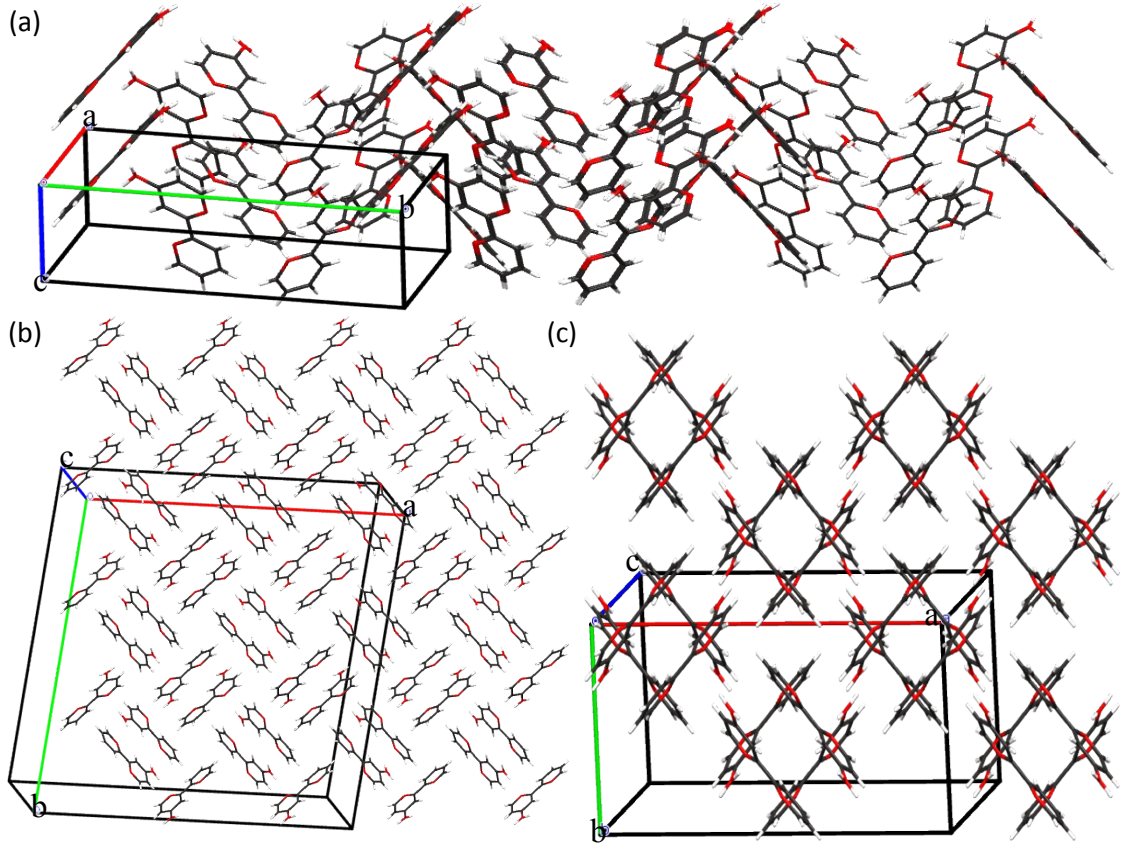

Figure S4: Two dimensional packing arrangements in (a) **AMBPY-I**, (b) **AMBPY-II** and (c) **AMBPY-III** respectively.

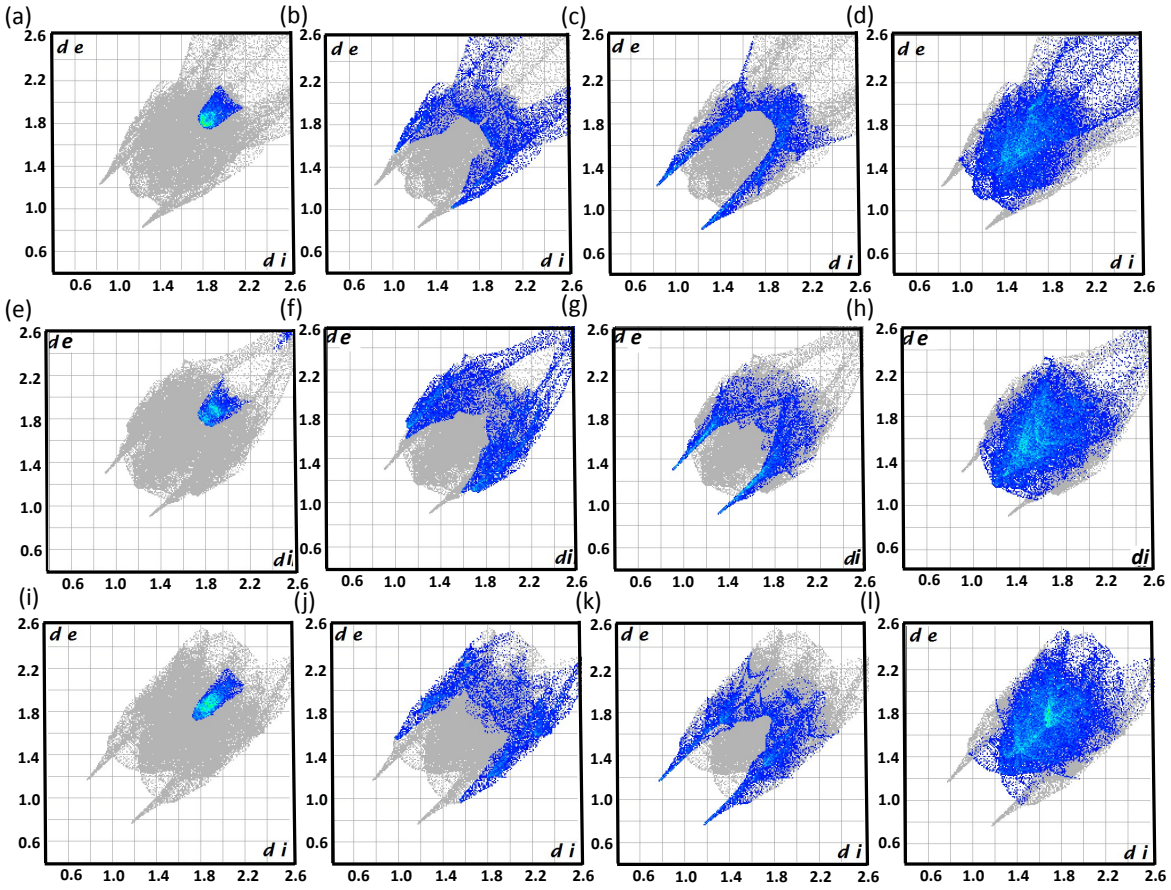

Figure S5: Two dimensional finger plots representing various interactions in **AMBPY** polymorphs. (a), (e), (i) correspond to C···C, (b), (f), (j) correspond to C···H, (c), (g), (k) correspond to N···H and (d), (h), (l) correspond to H···H interactions respectively (1st, 2nd and 3rd row represents **AMBPY-I**, **AMBPY-II** and **AMBPY-III** respectively).

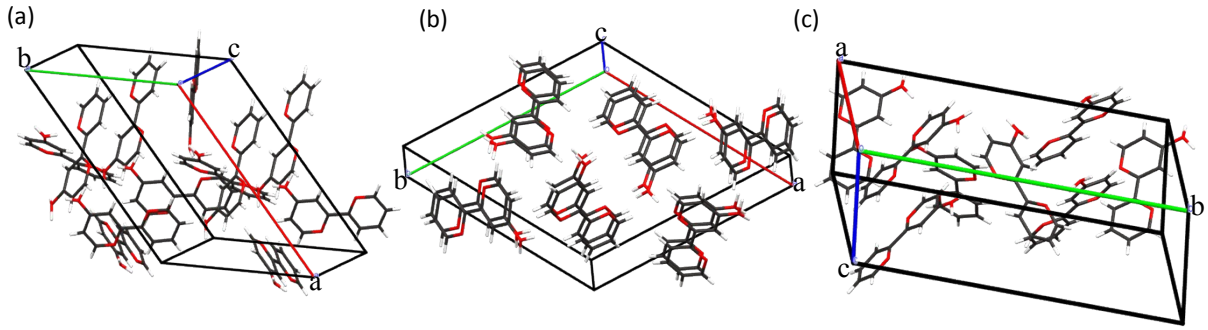

Figure S6: Close packing arrangements in **AMBPY-I** (γ-motif). (a) offset stacking along *b* axis, (b) face-to-face infinite stacking along *c* axis and (c) edge-to-face stacking along *a* axis.

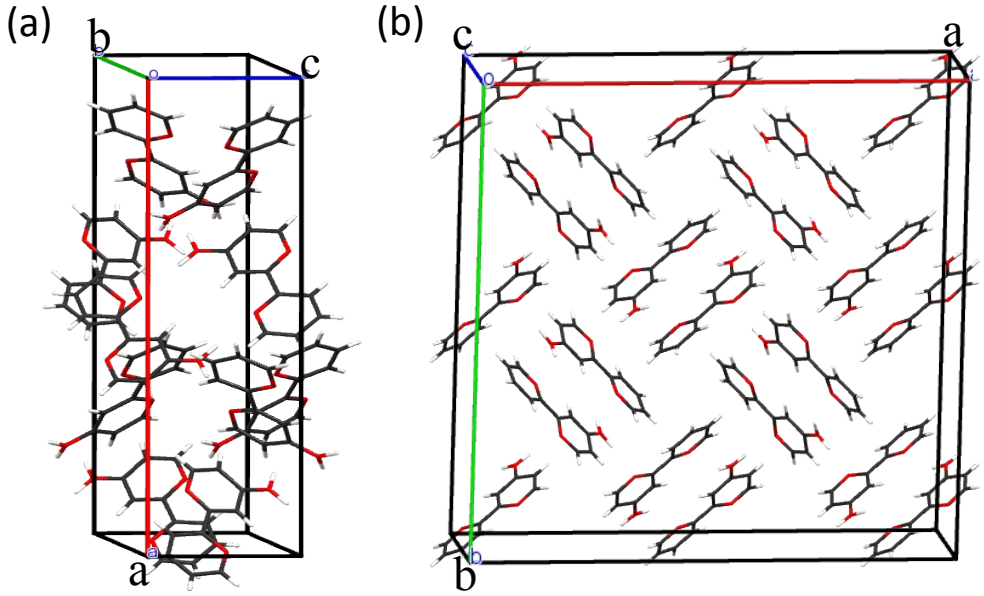

Figure S7: Close packing arrangements in **AMBPY-II** (sandwich herringbone). (a) offset stacking along *b* axis and (b) edge-to-face stacking along *c* axis.

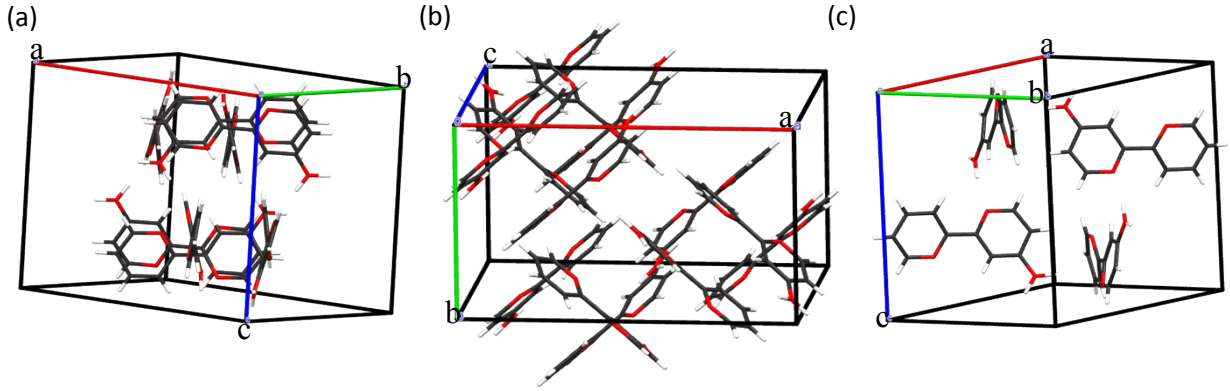

Figure S8: Close packing arrangements in **AMBPY-III** (γ- motif). (a) offset stacking along *a* axis, (b) face-to-face infinite stacking along *c* axis and (c) edge-to-face stacking along *b* axis.

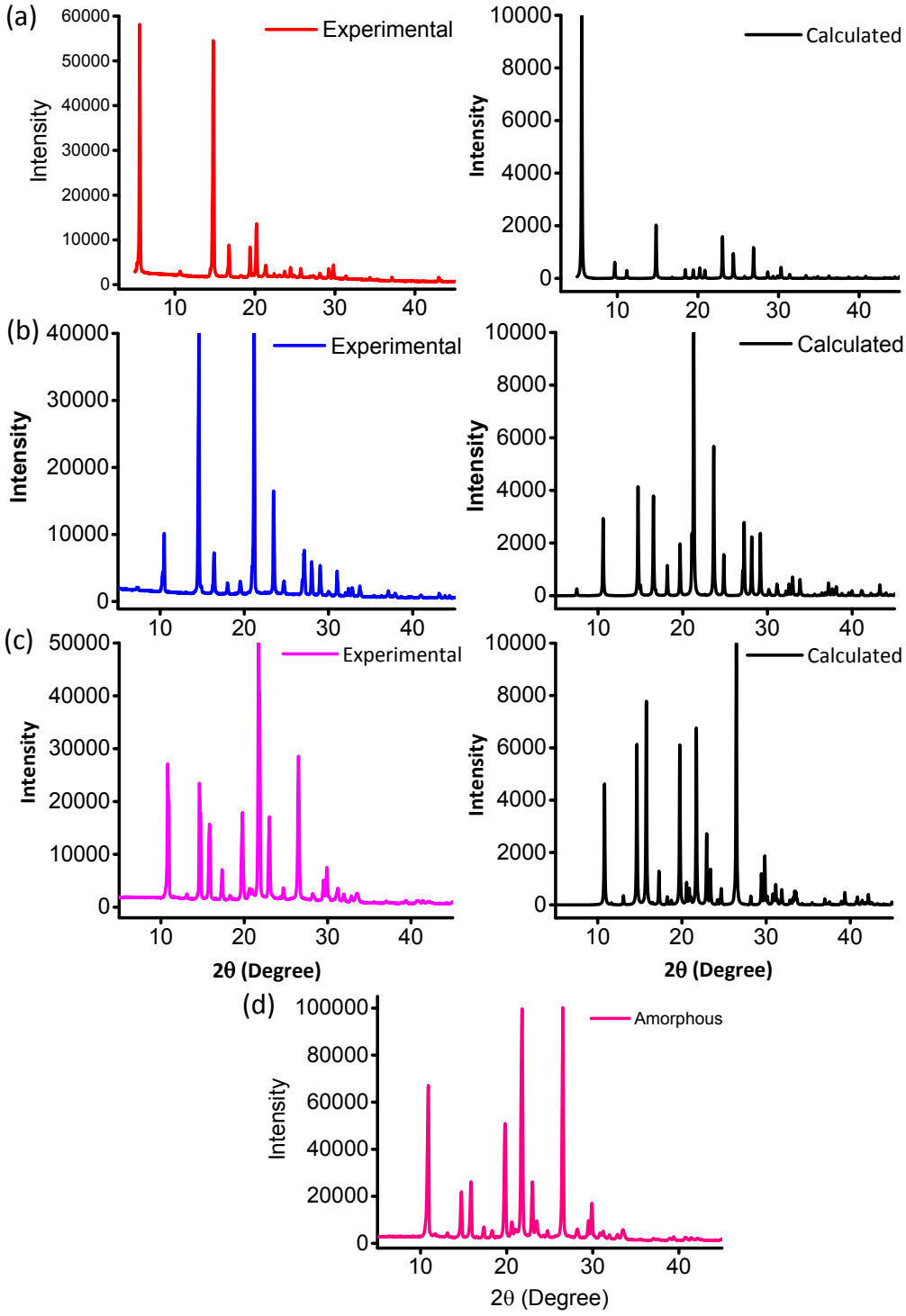

Figure S9: Comparison of experimental and calculated powder XRD pattern for **AMBPY** polymorphs (a) **AMBPY-I**, (b) **AMBPY-II** and (c) **AMBPY-III**. (d) PXRD pattern of amorphous **AMBPY**.

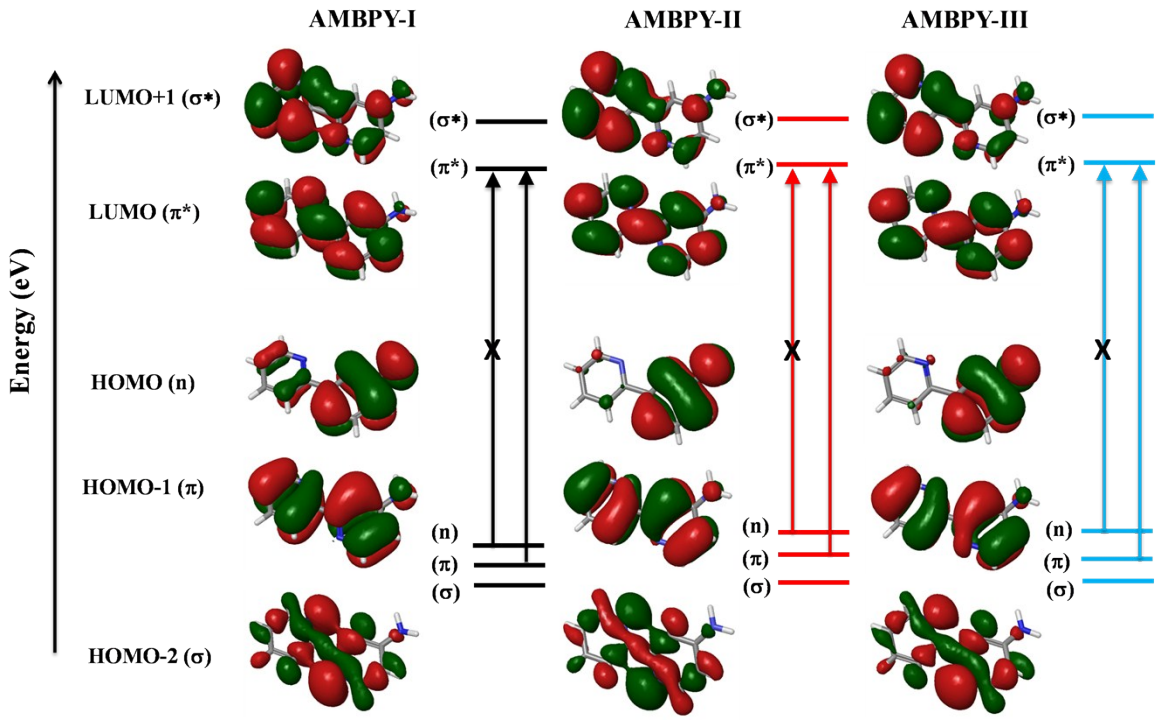

Figure S10: Frontier molecular orbital (FMO) analysis of **AMBPY** polymorphs calculated from B3LYP-D3/6-31G**+ level of theory from crystal structure in Schrödinger Materials Science Suite using Jaguar DFT engine.

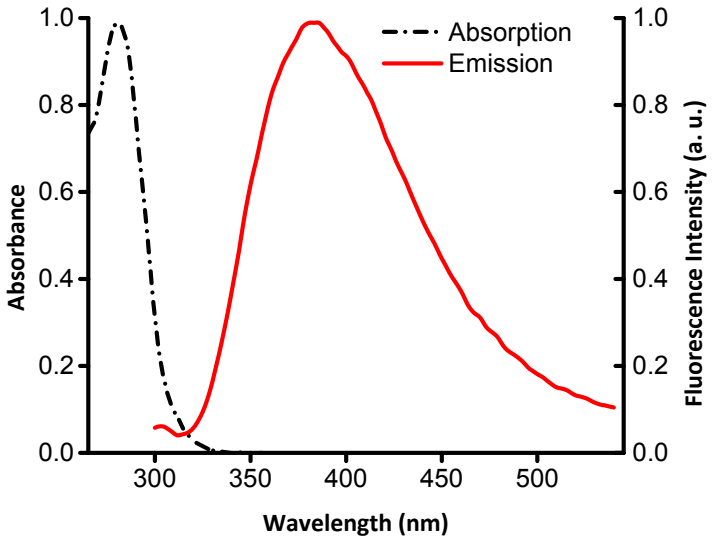

Figure S11: Absorption and emission (λ_{exc}= 290 nm) spectrum of **AMBPY** in $CHCl_3$.

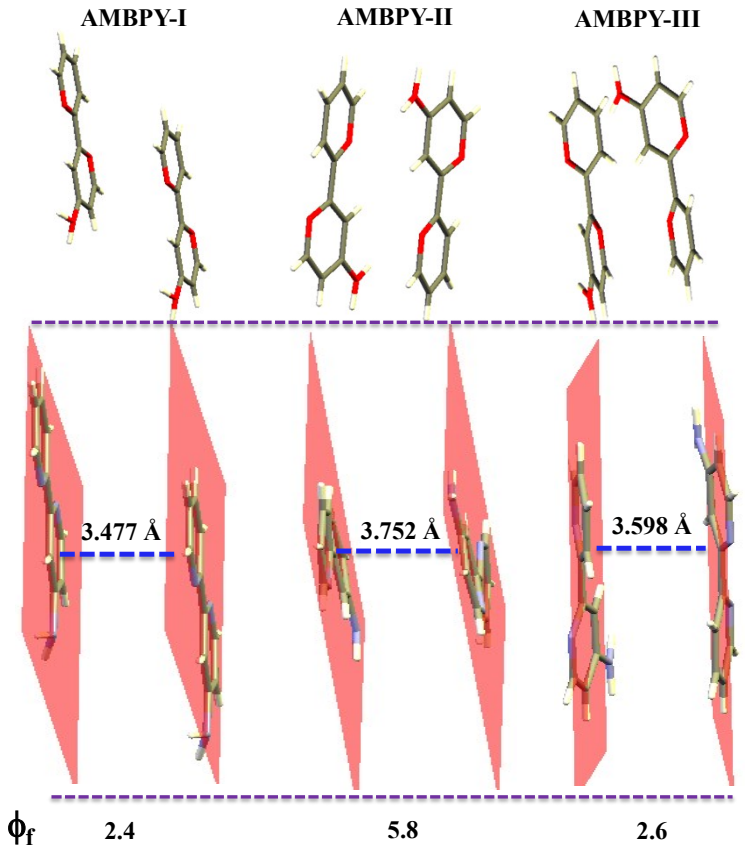

Figure S12: Describes distance of π-π separation observed in nearest neighbours of **AMBPY** polymorphs.

References:

1. J. R. Lakowicz, *Principles of Fluorescence Spectroscopy*, Springer, New York, 2006.
2. A. Spek, *Acta Cryst.C*, 2015, **71**, 9-18.
3. C. F. Macrae, P. R. Edgington, P. McCabe, E. Pidcock, G. P. Shields, R. Taylor, M. Towler and J. van de Streek, *J. Appl. Crystallogr.*, 2006, **39**, 453-457.
4. T. Smith and J. Guild, *Trans. Opt. Soc.*, 1931, **33**, 73.
5. (a) S. K. Wolff, D. J. Grinwood, J. J. McKinnon, M. J. Turner, D. Jayatilaka and M. A. Spackman, University of Western Australia, Perth, Australia, 2012; (b) M. A. Spackman and D. Jayatilaka, *CrystEngComm*, 2009, **11**, 19-32.
6. M. J. Frisch, G. W. Trucks, H. B. Schlegel, G. E. Scuseria, M. A. Robb, J. R. Cheeseman, G. Scalmani, V. Barone, B. Mennucci, G. A. Petersson, H. Nakatsuji, M. Caricato, X. Li, H. P. Hratchian, A. F. Izmaylov, J. Bloino, G. Zheng, J. L. Sonnenberg, M. Hada, M. Ehara, K. Toyota, R. Fukuda, J. Hasegawa, M. Ishida, T. Nakajima, Y. Honda, O. Kitao, H. Nakai, T. Vreven, J. A. Montgomery Jr., J. E. Peralta, F. Ogliaro, M. J. Bearpark, J. Heyd, E. N. Brothers, K. N. Kudin, V. N. Staroverov, R. Kobayashi, J. Normand, K. Raghavachari, A. P. Rendell, J. C. Burant, S. S. Iyengar, J. Tomasi, M. Cossi, N. Rega, N. J. Millam, M. Klene, J. E. Knox, J. B. Cross, V. Bakken, C. Adamo, J. Jaramillo, R. Gomperts, R. E. Stratmann, O.

Yazyev, A. J. Austin, R. Cammi, C. Pomelli, J. W. Ochterski, R. L. Martin, K. Morokuma, V. G. Zakrzewski, G. A. Voth, P. Salvador, J. J. Dannenberg, S. Dapprich, A. D. Daniels, Ö. Farkas, J. B. Foresman, J. V. Ortiz, J. Cioslowski and D. J. Fox, Gaussian, Inc., Wallingford, CT, USA, 2009.
7. A. D. Bochevarov, E. Harder, T. F. Hughes, J. R. Greenwood, D. A. Braden, D. M. Philipp, D. Rinaldo, M. D. Halls, J. Zhang and R. A. Friesner, *Int. J. Quantum Chem.*, 2013, **113**, 2110-2142.
8. Z. Zhou, G. H. Sarova, S. Zhang, Z. Ou, F. T. Tat, K. M. Kadish, L. Echegoyen, D. M. Guldi, D. I. Schuster and S. R. Wilson, *Chem. Eur. J.*, 2006, **12**, 4241-4248.